

Midgap states in corrugated graphene: Ab-initio calculations and effective field theory

T. O. Wehling,¹ A. V. Balatsky,² A. M. Tsvelik,³ M. I. Katsnelson,⁴ and A. I. Lichtenstein¹

¹*I. Institut für Theoretische Physik, Universität Hamburg, Jungiusstraße 9, D-20355 Hamburg, Germany*

²*Theoretical Division, Los Alamos National Laboratory, Los Alamos, New Mexico 87545, USA*

³*Department of Condensed Matter Physics and Materials Science,*

Brookhaven National Laboratory, Upton, NY 11973-5000, USA

⁴*Institute for Molecules and Materials, Radboud University of Nijmegen,*

Heijendaalseweg 135, 6525 AJ Nijmegen, The Netherlands

(Dated: November 5, 2018)

We investigate the electronic properties of corrugated graphene and show how rippling-induced pseudomagnetic fields alter graphene's low-energy electronic properties by combining first principles calculations with an effective field theory. The formation of flat bands near the Fermi level corresponding to pseudo-Landau levels is studied as a function of the rippling parameters. Quenched and relaxed ripples turn out to be fundamentally different in this respect: It is demonstrated, both numerically and analytically, that annealing of quenched ripples can destroy the flat bands.

Graphene, i.e. a monolayer of graphite, is the first truly two dimensional (2D) material available for experiments [1, 2]. Its low energy electronic structure resembling 2D Dirac massless fermion dynamics with the speed of light c being replaced by the Fermi velocity $v_f \approx c/300$ makes ultrarelativistic physics observable in this material [3, 4, 5]. These extraordinary electronic properties are immediately related to the graphene's 2D honeycomb crystal structure, which was puzzling itself: Thermal fluctuations in two-dimensional solids, in principle, should lead to huge displacements of the carbon atoms from their perfect lattice arrangement and destroy any long range crystalline order. As an important step towards solving this puzzle, transmission electron microscopy [6] and atomistic simulations [7] found that free standing graphene sheets are not perfectly flat but exhibit ripples. In addition to this intrinsic crumpling, graphene's bonding to a substrate can also introduce rippling [8, 9]. Both, the intrinsic and extrinsic ripples, may be accompanied by different strengths of in plane strain.

The effect of curvature and strain on the electronic structure of graphene can be described by effective gauge fields A acting on the electrons [10, 11] - in close analogy to curvature effects in carbon nanotubes (CNTs) [12, 13]. There, curvature decisively determines the low energy electronic properties, as it can open band gaps: The induced effective gauge fields shift the Fermi points of the 2D graphene bands away from the 1D nanotube bands. In graphene, on the contrary, the Dirac points are similarly shifted by uniform gauge fields but no gap opening is expected unless a modulated electrostatic potential is present [14]. Rather, the Dirac point shifting leads to unusually strong electron-phonon interactions [15].

However, the rippling induced gauge fields A are nonuniform and affect the electrons in graphene like an *effective* magnetic field $\mathcal{B} = \nabla \times A$ [10]. Tight-binding (TB) estimations on the effective magnetic field induced to graphene by rippling found the possibility of partially flat bands, which are the analog of Landau levels in real

magnetic fields [14]. Therefore, these flat bands are referred to as *pseudo* Landau levels. In particular, zero-energy chiral states ($n = 0$ LL) at the Fermi level should occur in inhomogeneous (real and effective) magnetic fields, as was pointed out from topological considerations [3, 16]. The appearance of ripple-induced mid-gap states can lead to important consequences: The increased DOS at the Fermi level will enhance the tendency to spatial inhomogeneities [14] as well as lead to strong resonant electron scattering [5, 17, 18]. Knowing the conditions under which midgap states occur is therefore essential to resolve the debate on electron scattering in graphene.

So far, the predictions on midgap states have been rather qualitative involving adjustable parameters, like hopping matrix elements, their change with strain and curvature as well as they neglected rehybridization effects of the π and σ bands. It is not clear *a priori* how essential these effects can be. For example, taking into account next-nearest-neighbor hopping leads to a *scalar* electrostatic potential induced by the ripples [19] which can cause opening a gap around the Fermi level [14]. Only based on complete first-principles calculations one can judge how important the corrections to the simplest nearest-neighbor TB model are.

In this letter, we present full potential density functional theory (DFT) studies of quenched and annealed graphene ripples. We find flat bands very close to the Dirac point for quenched ripples, whereas in annealed ripples these midgap states turn out to be suppressed. Based on a nearest neighbor TB model, we extend the low energy effective field theory description of graphene to include this relaxation effect. The qualitative agreement of our effective field theory with DFT justifies this nearest neighbor TB based theory for describing corrugated graphene.

In our DFT calculations, quenched ripples are modelled as sinusoidal graphene ripples with height field $h(x, y) = h_0 \sin(qx)$ (Fig. 1, upper panel). While the effective gauge field A is caused by strain and curvature,

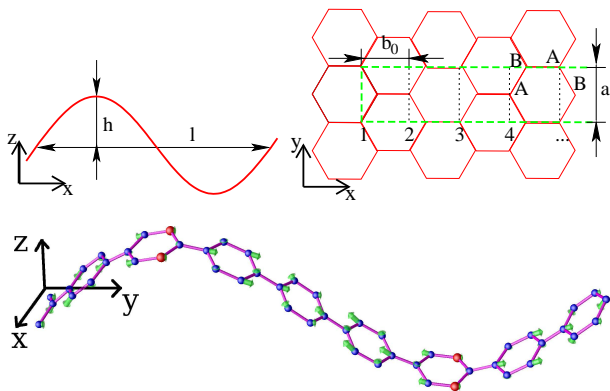


Figure 1: (Colour online) Upper panel: Schematic top and side view of the sinusoidal graphene ripples. The rippling period is denoted by l and their amplitude by h . Lower panel: Perspective view of a relaxed graphene ripple. The green arrows show the displacement of the atoms during the relaxation. To enforce a constant rippling amplitude the vertical position of the atoms marked as big red dots has been fixed.

the strain in the ripple can be significantly reduced by allowing all atoms and the supercell shape to relax with the constraint of fixed rippling amplitude h_0 . As starting point for the relaxed cell shape, we shortened the supercell in rippling direction such that the arc length of one sinusoidal graphene ripple period coincides with the equilibrium length of the same supercell for flat graphene. Then, standard relaxation of the atomic positions and the cell shape under the rippling constraint from above has been performed. This relaxation leads to our model of annealed graphene ripples, where "annealed" means that in these ripples possible external sources for energy barriers preventing the ripples from relaxation have been removed. Such sources might be impurities or bonding to a substrate with lattice mismatch.[20, 21]

In all of our calculations we employ the generalized gradient approximation (GGA) [22] to DFT for supercells containing up to 160 carbon atoms. The resulting Kohn-Sham problems are solved with the Vienna Ab Initio Simulation (VASP) [23] package by expanding the electronic bands into projector augmented waves (PAW) [24, 25]. Plane wave cut-offs of 500 eV for band-structure and 875 eV for the relaxations and total energy calculations were used. For the total energy calculations, the Brillouin zone integrations were performed with 0.1 eV Gaussian smearing on k-meshes denser than 24×24 when folded back to the graphene first Brillouin zone, whereas for relaxations and input charge densities for band structure calculations k-meshes diluted by a factor of 2 turned out to be sufficient.

Firstly, the occurrence of the $n = 0$ LL in quenched ripples as function of the ripple length l and h_0/l has been studied, in this way. For $h_0/l = 1\text{\AA}/4b_0$ with $b_0 = \sqrt{3}a_0/2$ and $a_0 = 2.465\text{\AA}$ being the graphene lattice constant, prominent changes in the high valance and

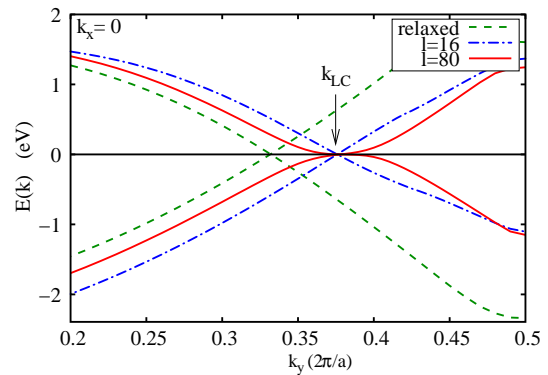


Figure 2: (Colour online) Band structure of corrugated graphene sheets: The highest valence and lowest conduction bands along the k_y direction (perpendicular to the rippling direction) are shown in main panel for different armchair ripples. Dash dotted and solid lines: Unrelaxed sinusoidal ripples with fixed $h_0/l = 1\text{\AA}/4b_0$ ratio for $l = 16, 80b_0$. Dashed lines: A ripple relaxed with the constraint $h_0 = 4\text{\AA}$ and a rippling period of 16 graphene unit cells. The energy required to create the quenched ripples considered, here, is 0.5 eV/atom. For the relaxed ripple this energy is 0.03 eV/atom

the low conduction bands occur (Fig. 2) depending on the rippling period l . The shorter ripple ($l = 16b_0$) exhibits electron dispersion resembling massless particles with the Dirac point shifted from $k_y = 2\pi/3a_0$ to $k_y \approx 0.375(2\pi/a_0)$, where k_y is the crystal momentum perpendicular to the rippling direction, x . However, the bands of the $l = 80b_0$ ripple are flat near the Fermi level and exhibit all characteristics of the $n = 0$ LL of Dirac fermions: They are chiral, that is, fully sublattice polarized and localized in regions of maximum effective magnetic field \mathcal{B} .

This manifests in the local density of states (LDOS) (see Fig. 3) as follows. For a ripple of the form $h(x, y) = h_0 \sin(qx)$ with $q = 2\pi/l$ and l sufficiently large, the effective gauge field is $A \sim (hq \cos(qx))^2$ and accordingly $\mathcal{B} \sim h^2 q^3 \sin(2qx)$. Thus, for $l = 80b_0$ the absolute value of the effective field is maximum around $x = 10, 30, 50, 70b_0$. In this high field region (see Fig. 3), the spectrum is gapped around the Fermi level ($E = 0$) in one sublattice (here B) but exhibits a mid-gap peak in the other sublattice. This will lead to sublattice stripes in low bias STM topographs with sublattice A bright and B dark, which is very reminiscent of midgap impurity states [26]. In the low effective field region, the LDOS recovers the pseudogap shape typical for flat graphene and the two sublattices appear fully equivalent again.

The band structures of the quenched ripples shown in Fig. 2 allow to estimate the strength of the involved pseudomagnetic fields: Given the shift of the Dirac point of $\delta k_y = 0.042(2\pi/a_0)$ away from the flat graphene value, we obtain the average gauge field $A_0 = \hbar \delta k_y / e = 2.8 \cdot 10^3 \text{ T} a_0$. Due to the sinusoidal shape

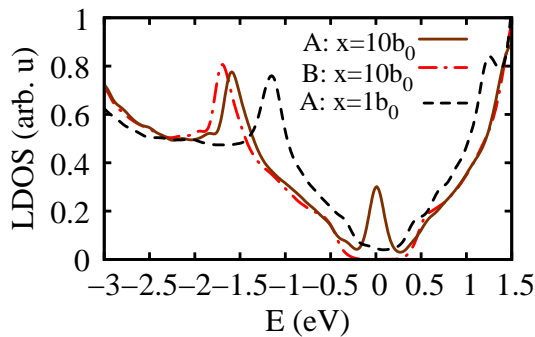


Figure 3: (Colour online) The local density of states (LDOS) inside the cells at $x = 1b_0$ (low eff. field) and at $x = 10b_0$ (high field region). For the low field region, the LDOS is the same in both sublattices (only sublattice A plotted is here, dashed line), whereas in the high field region the LDOS in sublattice A (solid) and B (dash-dotted) differ significantly.

of the ripple the amplitude sinusoidal pseudomagnetic field is $\mathcal{B}_0 = A_0 q \approx 250\text{T}$ for $q = 2\pi/80b_0$. Due to $\mathcal{B} = \mathcal{B}_0 \sin(2qx)$ a pseudo Landau level wave function should be localized on a length less than $l/4$ corresponding to an area of $l^2/16 = 18\text{nm}^2$. (See also Ref. [14].) 250T correspond to approx. 2 (pseudo)magnetic flux quanta per 18nm^2 .

The ripple under consideration has maximum local strain of 24%, which is more than the average strain of approx. 1% measured in epitaxial graphene[20] or 4% found in other nanosized epitaxial materials[27]. Scaling down the pseudo magnetic field to these strain values yields 10T and 40T, respectively.

So far, we considered quenched ripples, but the pseudomagnetic field is sensitive not only to flexural deformations but also to in-plane distortions. In general, ripples will be accompanied by in-plane distortions: For the quenched ripple of length $l = 16b_0$ with $h/l = 1\text{\AA}/4b_0$, we relaxed the atomic positions and the supercell shape of the ripple with the constraint of fixed rippling height. This "annealed" ripple is still sinusoidal (Fig. 1, lower panel) but with all nearest neighbor bond lengths being equal after relaxation. During this relaxation process the effective gauge field decreases as can be seen from the band structure of the relaxed ripple in Fig. 2. The Dirac point for the relaxed ripple is at $k_y \approx 0.332(2\pi/a_0)$, which is by a factor of 40 closer to the flat graphene value of $k_y = 1/3(2\pi/a_0)$ than the Dirac point of the quenched ripples. This corresponds to a decrease of the average effective gauge field the same factor. This suppression of effective gauge and pseudomagnetic fields in the annealed ripple can be understood in terms of the following model:

Consider the nearest neighbor TB Hamiltonian

$$H = \sum_k (A_k^+, B_k^+) \begin{pmatrix} 0 & t_{nn}(k) \\ \bar{t}_{nn}(k) & 0 \end{pmatrix} \begin{pmatrix} A_k \\ B_k \end{pmatrix}, \quad (1)$$

where t_{nn} are the hopping matrix elements and A_k (B_k)

the Fermi operators of electrons in sublattice A (B) with crystal momentum k . Close to $\pm\mathbf{K} = (0, \mp 4\pi/3\sqrt{3})$, in the corner of the Brillouin zone, the dispersion for the undeformed lattice vanishes linearly and a continuum theory describing low energy electronic states can be defined. As in Ref. [28], we introduce a pair of two-dimensional spinors $\Psi_1 = \begin{pmatrix} A_K \\ B_K \end{pmatrix}$, $\Psi_2 = \begin{pmatrix} B_{-K} \\ -A_{-K} \end{pmatrix}$ describing electronic wave packets centered at \mathbf{K} and $-\mathbf{K}$ point, respectively, and expand the hopping integrals. Near the \mathbf{K} point the undeformed hopping integral is

$$t_{nn}(\mathbf{k}) \approx \frac{3t_0 a_0}{2} (q_y - i q_x) \rightarrow 2v_0 \bar{\partial}, \quad (2)$$

where $q = k - K$, $\bar{\partial} = \frac{1}{2}(\partial_x + i\partial_y)$ and $v_0 = 3t_0 \tilde{a}_0/2$ is the Fermi velocity, involving explicitly the nearest-neighbor spacing $\tilde{a}_0 = a_0/\sqrt{3}$. Slow lattice deformations with the deformation tensor field

$$u_{ab} = \frac{1}{2}[\partial_a u_b + \partial_b u_a] + \partial_a h \partial_b h \quad (3)$$

with $a, b \in \{x, y\}$ lead to changes in the hopping integral

$$\delta t(\mathbf{Q}) / \left[\frac{\partial t_0}{\partial R} \right] = \sum_{\mu} e^{i\mathbf{Q}e_{\mu}} e_{\mu}^a \frac{\partial u^a}{\partial x^b} e_{\mu}^b = 3u_{zz} \quad (4)$$

where $e_1 = (1, 0)$, $e_2 = (1/2, \sqrt{3}/2)$, $e_3 = (1/2, -\sqrt{3}/2)$ are vectors connecting nearest neighbor sites and $z = x + iy$. Thus the nearest neighbor hopping matrix element near the point \mathbf{K} is now

$$2v_0 (\bar{\partial} - \gamma u_{zz}) \quad (5)$$

where $\gamma = \partial \ln t_0 / \partial R$ plays a role of the charge, and u_{zz} can be interpreted as a vector potential:

$$\bar{A}^3 = u_{zz}, A^3 = A_z^3 = A_x^3 - iA_y^3 = u_{z\bar{z}} \quad (6)$$

We have considered smooth lattice deformations and established that they generate an Abelian vector potential having opposite signs for different valleys. It is worth noticing that this vector potential constitutes a part of the non-Abelian field whose other noncommuting components $A^{1,2}$ are generated by abrupt changes of the nearest neighbor hopping integrals. The complete low energy Hamiltonian is [28]

$$H = \Psi^+ \{ I \otimes IA_0 + v_0 \sigma_{\mu} \otimes [-i\mathbb{1}\partial_{\mu} + \gamma \tau^a A_{\mu}^a] \} \Psi \quad (7)$$

where the Pauli matrices σ_{μ} , $\mu = x, y$ act in the spinor space and matrices τ^a , $a = 1, 2, 3$ act on the valley index of the spinor $\Psi^+ = (\Psi_1^+, \Psi_2^+)$.

The zero energy wave functions for the vector potential deformations can be found analytically for $A_0 = 0$. For simplicity we will restrict ourselves to the case of slow deformations when $A^{1,2} = 0$. Then the zero energy wave

functions (if they exist) are expressed in terms of pseudo-magnetic field

$$\mathcal{B} = i(\partial A^3 - \bar{\partial} \bar{A}^3) \quad (8)$$

For $\mathcal{B} > 0$ we have:

$$A_K = A_{-K} = z^n \exp\left[-\frac{\gamma}{\partial \bar{\partial}} \mathcal{B}\right], \quad B_K = B_{-K} = 0 \quad (9)$$

and for $\mathcal{B} < 0$ one has to interchange A_K, A_{-K} with B_K, B_{-K} and z with \bar{z} . The power n ranges from 0 to the integer part of the pseudomagnetic flux. As many zero modes exist.

The expression for \mathcal{B} and for the deformation tensor changes drastically depending on whether the elastic energy is at its minimum or not. The expression for the elastic energy density of a smooth surface compatible with the C_3 symmetry is given by [29]

$$\begin{aligned} E &= (\lambda + \mu) \left[\frac{1}{2} (\bar{\partial} u + \partial \bar{u}) + \partial h \bar{\partial} h \right]^2 \\ &\quad + \mu [\partial u + (\partial h)^2] [\bar{\partial} \bar{u} + (\bar{\partial} h)^2] + \frac{K}{2} (\nabla^2 h)^2 \\ &= \mu A \bar{A} + (\lambda + \mu) \left[\frac{1}{2 \partial \bar{\partial}} (\bar{\partial}^2 A + \partial^2 \bar{A}) + \frac{1}{\partial \bar{\partial}} \mathcal{R}[h] \right]^2 \\ &\quad + \frac{K}{2} (\nabla^2 h)^2 \end{aligned} \quad (10)$$

where $\mathcal{R} = [\partial^2 h \bar{\partial}^2 h - (\partial \bar{\partial} h)^2]$ is the Gaussian curvature of the surface. If the membrane is at equilibrium, the elastic energy (10) is at its minimum and the vector potential is given by

$$A^3 = -\frac{(\lambda + \mu)}{(\lambda + 2\mu)} \frac{\partial^2}{\partial \bar{\partial}} \mathcal{R}. \quad (11)$$

\mathcal{R} is the Jacobian of the coordinate transformation $\xi = \partial h$, $\bar{\xi} = \bar{\partial} h$:

$$\partial^2 h \bar{\partial}^2 h - (\partial \bar{\partial} h)^2 = \frac{\partial(\xi, \bar{\xi})}{\partial(z, \bar{z})} \quad (12)$$

Thus, \mathcal{R} and, as a consequence, A^3, \bar{A}^3 as well as A_0 vanish on any configuration of h which depends on just one Cartesian coordinate. This includes all plane wave configurations, in particular those studied by DFT in this letter.

Substituting Eqn. (11) into (8) we get

$$\mathcal{B} = \frac{i(\lambda + \mu)}{\lambda + 2\mu} \frac{\partial^3 - \bar{\partial}^3}{(\partial \bar{\partial})^2} [\partial^2 h \bar{\partial}^2 h - (\partial \bar{\partial} h)^2], \quad (13)$$

which is C_3 symmetric, as it must be. This C_3 symmetry of \mathcal{B} for a relaxed membrane leads to important qualitative differences with a real magnetic field. A local vortex of magnetic field with flux N carries N normalizable zero modes, but to create such a flux by deforming

a membrane is not possible. An analogue of a magnetic vortex is a point-like defect $h = h(|\mathbf{r} - \mathbf{a}|)$ carrying local Gaussian curvature $\mathcal{R} = \mathcal{R}(|\mathbf{r} - \mathbf{a}|)$. Then the argument in wave function (9) is $\frac{\gamma}{\partial \bar{\partial}} \mathcal{B} = \gamma \sin(3\phi) b(|r - a|)$, where $b(r) = \int \frac{dk}{(2\pi)^k} J_3(kr) \mathcal{R}_k$ and ϕ is the angle with respect to the crystalline axis. Since \mathcal{R}_k is constant at small k , at distances larger than the size of the defect $b(r) \sim r$. Such wave function is not normalizable. On the other hand the wave function with two defects with curvature of the opposite sign will be normalizable for the entire volume (as a plane wave). Such state is non-degenerate, that is we have $n = 0$ in (9). So, if we allow the graphene membrane to relax there are only nondegenerate zero modes, which only exist for membrane configurations with nonzero Gaussian curvature. Therefore, the effect of relaxations on the electronic properties of the graphene ripples is qualitatively the same for 1D and 2D ripples. The *degenerate* zero modes are suppressed in relaxed ripples and no significant midgap peak in the total DOS of 2D ripples is expected to occur.

In conclusion, our results demonstrate an essential difference between quenched and annealed ripple structure. If the system is allowed to relax to its minimum of elastic energy for a given $h(x, y)$ profile it decreases drastically the amplitude of pseudo-magnetic fields and can lead to disappearance of the mid-gap states. It may be an important statement in light of the hypothesis [17] that *quenched* ripples are the main source of scattering in graphene and the very recent observation that annealing of a freely hanged graphene membrane can increase drastically its mobility [30]: Upon annealing, impurities causing energy barriers that prevent the suspended graphene from relaxation might be removed. This issue requires further investigations. Our ab-initio calculations reveal a perfect particle-hole symmetry at low energies and justify the nearest neighbor hopping based field theory for describing the electronic properties of graphene ripples.

The authors are thankful to A. Geim, K. Novoselov, and I. Aleiner for inspiring discussions. This work was supported by SFB 668 (Germany), FOM (The Netherlands) and DOE at Los Alamos. The authors acknowledge computer time from LANL (USA) and HLRN (Germany). T.O.W. is grateful to LANL for hospitality during the visit, when the ideas presented in this work were set off. A.M.T. acknowledges the support from US DOE under contract number DE-AC02 -98 CH 10886.

-
- [1] K. S. Novoselov, A. K. Geim, S. V. Morozov, D. Jiang, Y. Zhang, S. V. Dubonos, I. V. Grigorieva, and A. A. Firsov, *Science* **306**, 666 (2004).
 - [2] K. S. Novoselov, D. Jiang, F. Schedin, T. J. Booth, V. V. Khotkevich, S. V. Morozov, and A. K. Geim, *PNAS* **102**, 10451 (2005).
 - [3] K. S. Novoselov, A. K. Geim, S. V. Morozov, D. Jiang,

- M. I. Katsnelson, I. V. Grigorieva, S. V. Dubonos, and A. A. Firsov, *Nature* **438**, 197 (2005).
- [4] Y. Zhang, Y.-W. Tan, H. L. Stormer, and P. Kim, *Nature* **438**, 201 (2005).
- [5] M. I. Katsnelson and K. S. Novoselov, *Solid State Commun.* **143**, 3 (2007).
- [6] J. C. Meyer, A. K. Geim, M. I. Katsnelson, K. S. Novoselov, T. J. Booth, and S. Roth, *Nature* **446**, 60 (2007).
- [7] A. Fasolino, J. H. Los, and M. I. Katsnelson, *Nature Mater.* **6**, 858 (2007).
- [8] E. Stolyarova, K. T. Rim, S. Ryu, J. Maultzsch, P. Kim, L. E. Brus, T. F. Heinz, M. S. Hybertsen, and G. W. Flynn, *PNAS* **104**, 9209 (2007).
- [9] M. Ishigami, J. Chen, W. Cullen, M. Fuhrer, and E. Williams, *Nano Lett.* **7**, 1643 (2007).
- [10] S. V. Morozov, K. S. Novoselov, M. I. Katsnelson, F. Schedin, L. A. Ponomarenko, D. Jiang, and A. K. Geim, *Phys. Rev. Lett.* **97**, 016801 (2006).
- [11] A. F. Morpurgo and F. Guinea, *Phys. Rev. Lett.* **97**, 196804 (2006).
- [12] C. L. Kane and E. J. Mele, *Phys. Rev. Lett.* **78**, 1932 (1997).
- [13] P. E. Lammert and V. H. Crespi, *Phys. Rev. B* **61**, 7308 (2000).
- [14] F. Guinea, M. I. Katsnelson, and M. A. H. Vozmediano, *Phys. Rev. B* **77**, 075422 (2008).
- [15] S. Pisana, M. Lazzeri, C. Casiraghi, K. S. Novoselov, A. K. Geim, A. C. Ferrari, and F. Mauri, *Nat. Mater.* **6**, 198 (2007).
- [16] M. I. Katsnelson and M. F. Prokhorova, *Phys. Rev. B* **77**, 205424 (2008).
- [17] M. I. Katsnelson and A. K. Geim, *Phil. Trans. R. Soc. A* **366**, 195 (2007).
- [18] T. Stauber, N. M. R. Peres, and F. Guinea, *Phys. Rev. B* **76**, 205423 (2007).
- [19] A. H. Castro Neto and E.-A. Kim (2007)), arXiv:cond-mat/0702562 (unpublished).
- [20] J. Röhrli, M. Hundhausen, K. V. Emtsev, T. Seyller, R. Graupner, and L. Ley, *Appl. Phys. Lett.* **92**, 201918 (pages 3) (2008).
- [21] P. Lauffer, K. V. Emtsev, R. Graupner, T. Seyller, L. Ley, S. A. Reshanov, and H. B. Weber, *Phys. Rev. B* **77**, 155426 (pages 10) (2008).
- [22] J. P. Perdew, J. A. Chevary, S. H. Vosko, K. A. Jackson, M. R. Pederson, D. J. Singh, and C. Fiolhais, *Phys. Rev. B* **46**, 6671 (1992).
- [23] G. Kresse and J. Hafner, *J. Phys.: Condes. Matter* **6**, 8245 (1994).
- [24] G. Kresse and D. Joubert, *Phys. Rev. B* **59**, 1758 (1999).
- [25] P. E. Blöchl, *Phys. Rev. B* **50**, 17953 (1994).
- [26] T. O. Wehling, A. V. Balatsky, M. I. Katsnelson, A. I. Lichtenstein, K. Scharnberg, and R. Wiesendanger, *Phys. Rev. B* **75**, 125425 (2007).
- [27] H. Brune, M. Giovannini, K. Bromann, and K. Kern, *Nature* **394** (1998).
- [28] M. S. Foster and I. Aleiner, *Phys. Rev. B* **77**, 195413 (2008).
- [29] D. Nelson, T. Piran, and S. Weinberg, eds., *Statistical Mechanics of Membranes and Surfaces* (World Scientific, Singapore, 2004).
- [30] K. I. Bolotin, K. Sikes, Z. Jiang, M. Klima, G. Fudenberg, J. Hone, P. Kim, and H. Stormer, *Solid State Commun.* **146**, 351 (2008).